

Brownian-dynamics simulations of melting of finite two-dimensional systems with logarithmic interaction

A. T. Fiory

Bell Laboratories, Murray Hill, New Jersey 07974

(Received 22 March 1983)

Finite-size, two-dimensional one-component Coulomb systems (charged rods) with a circular free boundary were simulated by Brownian equation-of-motion dynamics. Positional- and orientational-order correlation functions, site-coordination defects, and particle displacements were examined as a function of the coupling constant $\Gamma = q^2/k_B T$ for samples of 253 and 583 particles. Melting of single-crystal samples occurs as increasing disorder with decreasing Γ without a conspicuous feature in the Γ dependence of order parameters. A transition between hexaticlike and isotropic fluid phases is identified at $\Gamma \approx 148$ for the 583-particle sample and $\Gamma \approx 153$ for the 253-particle sample. Results are compared with Monte Carlo and molecular-dynamics simulations and the theory of dislocation-mediated melting of lattices of quantized vortices.

I. INTRODUCTION

Computer simulations of melting in two-dimensional lattices by either Monte Carlo or molecular-dynamics techniques have been carried out by various authors on several model pair potentials.¹ The logarithmic potential appropriate for the interaction between charged rods is used in the present computer experiment, and was also recently examined by Caillol *et al.*² with Monte Carlo and by de Leeuw and Perram³ with molecular dynamics. Although the results of several simulations agree with the theory of continuous melting,⁴ others show evidence for a first-order transition, such as thermal hysteresis and two-phase equilibrium.

Various mechanisms of melting have been considered theoretically. Nelson and Halperin⁴ used the ideas of Kosterlitz and Thouless⁵ in their theory which predicts that melting may occur by two second-order phase transitions driven by dislocation-pair unbinding and disclination-pair unbinding, with an intermediate liquid-crystalline hexatic phase. Other theories of melting considered the grain boundary mechanism⁶ and first-order processes.⁷ It is worth noting one finding for several simulations, that the magnitude of the shear modulus at melting is in agreement with the universality prediction derived from the renormalization-group theory.^{1,8,9}

In the present work Brownian-motion dynamics is used, as a variant of the molecular-dynamics technique, to study the melting of a two-dimensional Coulomb system with a free boundary. In addition to the very "soft" interaction potential, this approach may increase the ability of the simulated system to reach equilibrium with respect to disclination and dislocation motion.¹⁰ Restriction to finite length by an explicit sample boundary can be complementary to the finite running time in a simulation. Although there is no determination as to whether this equilibrium criterion is satisfied, the present simulations find a hexaticlike fluid phase and a transition to an isotropic phase. Despite the absence of critical temperatures in a finite system, the properties of the observed cooperative phenomena and the influence of sample size are obtained. Theoretical size effects were recently presented by Dutta and Sinha.¹¹

Two-dimensional Coulomb charges embedded in a viscous medium are analogs of quantized vortices in a superfluid film. Hydrodynamic stability of a vortex lattice was investigated theoretically by Fetter and Hohenberg, who showed that the system has a well-defined shear modulus.¹² The introduction of damping has no fundamental effect other than facilitating observation, as shown by Packard for vortices in superfluid helium.¹³ The high friction limit, considered in the present simulation, is generally applicable to superconducting films, owing to the finite conductivity of the normal metal and the finite size of the vortex core. Pearl¹⁴ was the first to show the logarithmic interaction potential between Abrikosov vortices in superconducting films and Conen and Schmid¹⁵ have calculated the shear modulus of vortex lattices. Theory for melting of vortex lattices has been given by Huberman and Doniach¹⁶ and by Fisher¹⁷ who had also estimated the renormalization of the shear modulus. The melting temperature found in the simulations lies within the range of values estimated by Fisher and agrees with the impedance transition temperature found for vortex lattices in aluminum films.¹⁸ The present work has some analogies to the treatment of vortex arrays in rotating superfluid helium by Campbell and Ziff,¹⁹ although the dynamics and boundary effects differ.

II. METHODOLOGY

A. Diffusion dynamics

The particles in the simulation emulate N infinitely long parallel charged rods embedded in a viscous medium. There is a uniform compensating charge of opposite sign extending over a circle of radius R . Since certain details of the particle dynamics, for example, the particle mass, do not effect the equation of state, it can be expected that Brownian-motion dynamics would produce results fundamentally similar to those of usual molecular dynamics. However, an important difference is that here energy is exchanged with the medium, so that the total energy of the ensemble of particles fluctuates with time and is not a constant of motion.

The inertial term in the equation of motion for the particles is omitted in the frequency range of interest, the high-friction limit, so that for each particle in the system

$$\frac{d\vec{r}_i}{dt} = \mu \vec{f}_i, \quad (2.1)$$

where \vec{r}_i is the position coordinate, μ the individual-particle mobility in the medium, and \vec{f}_i the driving force. The pair interaction contribution to the force is given as

$$\vec{f}_{ij} = q^2 \frac{\vec{r}_i - \vec{r}_j}{|\vec{r}_i - \vec{r}_j|^2}. \quad (2.2)$$

For vortices in superconductors, the relationship to microscopic parameters is given by

$$q^2 = \pi^2 \hbar^2 n_s / 2m, \quad (2.3)$$

where n_s is the areal density of superelectrons and m their mass. Again making connection to the superconductor, Eq. (2.2) implicitly assumes that the range of allowed particle separations satisfies the criteria

$$r_c < |\vec{r}_i - \vec{r}_j| < \Lambda, \quad (2.4)$$

where r_c is the core radius and $\Lambda = mc^2 / 2\pi n_s e^2$ the screening length that cuts off the interaction in a charged superfluid. Friction in vortex motion arises from normal electrical resistance.

It thus follows from Eq. (2.2) that the density of a collection of particles is irrelevant and the system is characterized by a dimensionless coupling constant,

$$\Gamma = q^2 / k_B T. \quad (2.5)$$

Treating an ensemble of particles which forms a two-dimensional lattice by the method of periodic boundary conditions, popular for simulating an infinite medium, can lead to metastable states which are misoriented and contain trapped defects. This is avoided here by choosing a finite-disc geometry for the N particles. The driving force on particle i in the system is then given by

$$\vec{f}_i = \sum_{\substack{j=1 \\ j \neq i}}^N q^2 \frac{\vec{r}_i - \vec{r}_j}{|\vec{r}_i - \vec{r}_j|^2} + \vec{f}_M + \vec{f}_L(t). \quad (2.6)$$

A central force \vec{f}_M from the oppositely-charged background, given as

$$\vec{f}_M = \begin{cases} -Nq^2 \vec{r}_i / R^2, & |\vec{r}_i| < R \\ -Nq^2 \vec{r}_i / |\vec{r}_i|^2, & |\vec{r}_i| > R \end{cases} \quad (2.7)$$

constrains the particles to remain in the disc, with free motion permitted along the boundary. The origin is at the center of the disc. $\vec{f}_L(t)$ is the random Langevin thermal force obeying the fluctuation-dissipation theorem.

Since the velocities are proportional to the instantaneous forces, the particle displacements after a time step Δt in the simulation are obtained by multiplying the first two terms in Eq. (2.6) by $\mu \Delta t$. Random walk displacements contributed by $\vec{f}_L(t)$ obey a Gaussian distribution of covariance

$$\sigma^2 = 2\mu \Delta t k_B T = 2\mu q^2 \Delta t / \Gamma. \quad (2.8)$$

Thus the length σ is the natural scale of the size of the steps used in the simulation. A fixed time step Δt was chosen so that σ is small compared to the interparticle spacing, although σ^2 varies with Γ . At the isotropic phase transition, the choice of parameters yields

$$\sigma^2 N / \pi R^2 \approx 2 \times 10^{-3}. \quad (2.9)$$

In the diffusion-controlled system there is no relevant Einstein period, which sets the size of the time step in molecular-dynamics simulations, since there are no propagating collective excitations. Hence Δt can be effectively much larger than the value used in usual molecular-dynamics simulations. The total running time at a given Γ , after an allowance for a settling time, was varied from 1024 to 4096 time steps, although most of the runs were for 1024 steps. Thus particle diffusion comparable to the interparticle spacing was observed, but long-range diffusion, lengths comparable to R , was not. The dynamics algorithm follows the usual practice of displacing all particles at each time step. Only potential energy may be calculated, since particle velocities are not determined.

B. Structure functions

Two system sizes were simulated, for $N=253$ and 583. These numbers were selected so that the unrelaxed triangular lattices, arrays fitting within a circle of radius R , have nearly regular polygon perimeters. The two-dimensional crystal obtained after the perfect triangular lattice has been allowed to relax at low temperature, or large Γ , is shown in Fig. 1. Deviations from a triangular

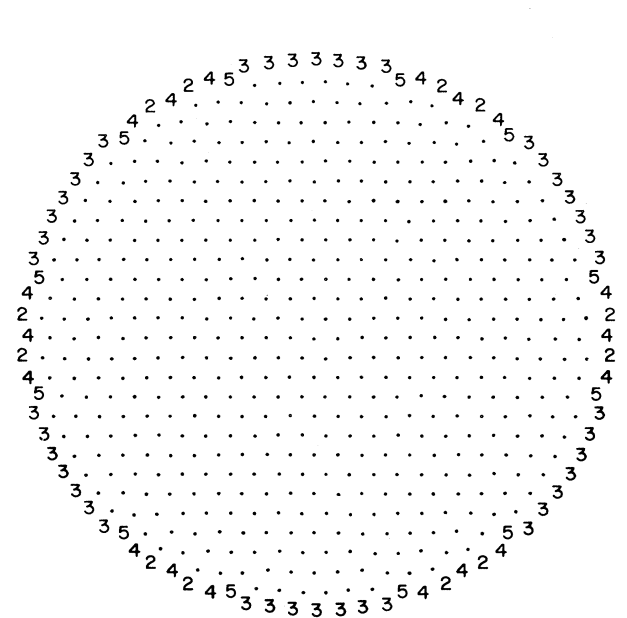


FIG. 1. 583-particle Coulomb crystal at low temperature, $\Gamma=10^4$. Particle positions with 6-fold coordination are represented by dots, other coordinations by numerals.

lattice occur mainly at the perimeter, which tends to form a circle. Thus the sample is viewed as a single crystal with localized boundary defects.

To classify the defects, the Voronoi polygon construction was used to obtain the local coordination number of z_i at each site.²⁰ Sites where z_i differs from 6 are shown by numerals in the figure. Except for the perimeter, sites with 5- or 7-fold coordination may be identified as disclinations. Near-neighbor 5-7 pairs are dislocations. To characterize the defect density, the following defect-count parameter is used:

$$\rho_d = N^{-1} \sum_i (z_i - \bar{z}_i)^2, \quad (2.10)$$

where z_i are the site coordinations and \bar{z}_i is taken to be 3 on the perimeter and 6 everywhere else. The average of $(z_i - \bar{z}_i)$ need not be zero, even though $\langle z_i - 6 \rangle = 0$ for unbounded arrays in two dimensions.

The pair correlation function is computed as a histogram whose elements are given by

$$g^{(k)}(r_k) = \sum_{\substack{i,j \\ i \neq j}} \Delta(r_k - |\vec{r}_i - \vec{r}_j|, \delta r) / p_0(r_k, \delta r), \quad (2.11)$$

where $\delta r = 2R/N$, $r_k = k \delta r$, $k = 1, 2, \dots, N$ and $\Delta(r, \delta r)$ a unit window function of width δr centered at $r = 0$. $p_0(r, \delta r)$ is the uniform distribution, which was obtained in a separate computation for the disc geometry. The statistical weight, which decreases to zero at $r = 2R$, is then normalized out. The result for a simulated $N = 583$ crystal at $\Gamma = 526$ is plotted in Fig. 2, where the points are connected by a continuous line. An average over 64 time samples was taken. Although the envelope of $g(r)$ decays slowly towards unity, the decay is in fact more rapid than the algebraic decay $r^{-\eta}$ with $\eta \leq 0.25$ predicted by theory for a stable infinite two-dimensional crystal.^{4,11} The decay length for $g(r)$ in this finite crystal is approximately $\xi_g = 0.7R$, determined as the length for decay by a factor of e . Peaks in $g(r)$ in the vicinity of $r \sim 2R$ reflect the tendency of the particles on the perimeter to form a circle and the near neighbors within a concentric circle. The following amplitude is later used to summarize the positional order correlations:

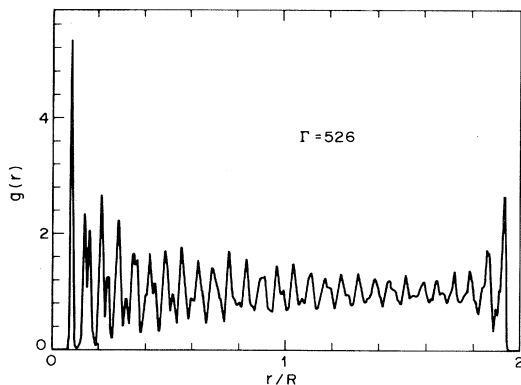


FIG. 2. Particle position pair correlation function at $\Gamma = 526$ vs separation in units of sample radius.

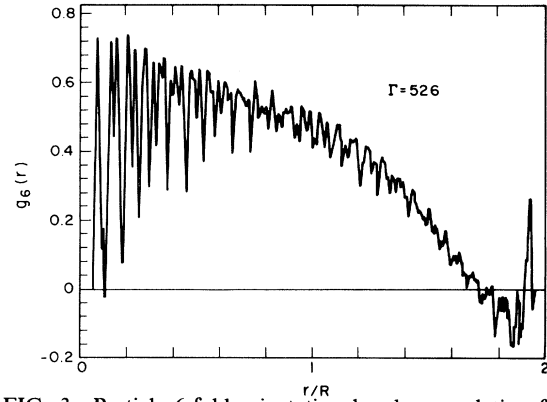


FIG. 3. Particle 6-fold orientational order correlation function vs reduced separation.

$$A_g = N^{-1} \sum_k |g^{(k)}(r_k) - 1|. \quad (2.12)$$

6-fold orientational order is represented by the bond-order parameter,

$$\psi_i(\vec{r}_i) = z_i^{-1} \sum_{j=1}^{z_i} e^{6i\theta_{ij}}, \quad (2.13)$$

where the sum extends over the z_i neighbors and θ_{ij} are the angles subtended by $(\vec{r}_i - \vec{r}_j)$ with respect to an arbitrary, fixed direction. The orientation correlation function is computed by averaging $\psi^* \psi$ over all pairs of particles:

$$g_6^{(k)}(r_k) = \frac{\left[\sum_{\substack{i,j \\ i \neq j}} \psi_i^*(\vec{r}_i) \psi_j(\vec{r}_j) \Delta(r_k - |\vec{r}_i - \vec{r}_j|, \delta r) \right]}{\sum_{\substack{i,j \\ i \neq j}} \Delta(r_k - |\vec{r}_i - \vec{r}_j|, \delta r)}. \quad (2.14)$$

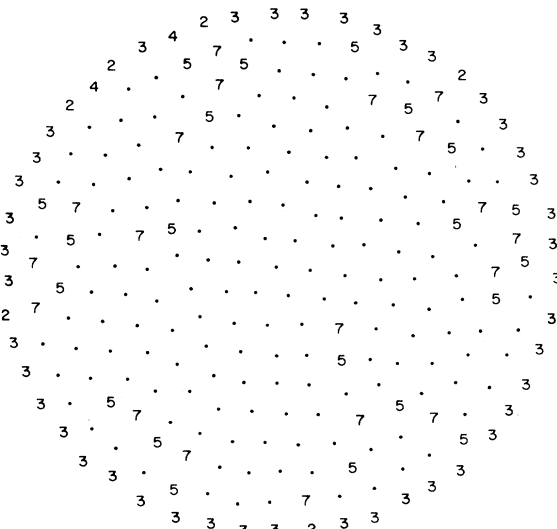


FIG. 4. 253-particle system at $\Gamma = 200$.

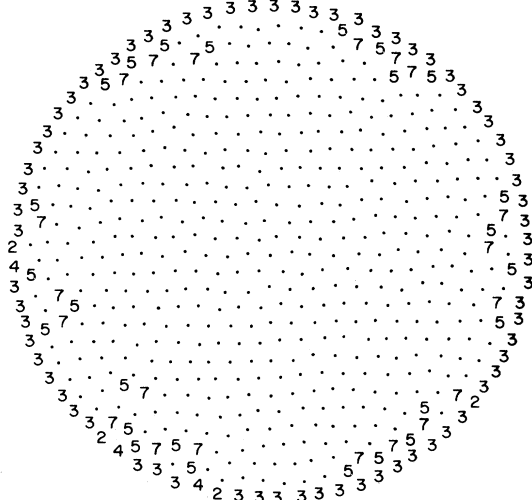


FIG. 5. 583-particle system at $\Gamma=200$, equivalent temperature as Fig. 4.

The result for g_6 at $\Gamma=526$ is shown in Fig. 3. The pronounced decrease in the peak heights with increasing r is a consequence of the boundary alignment, a significant departure from the constant value obtained for systems with periodic boundary conditions.^{1,20} An amplitude of hexatic order is defined as

$$A_{g_6} = N^{-1} \sum_k g_6^{(k)}(r_k). \quad (2.15)$$

The results presented in Figs. 1–3 are representative of the well-ordered particle arrangements obtained at large Γ , where the samples are manifestly single crystals. In the next section results encompassing the melting transition are presented.

III. Γ DEPENDENCE

The number of thermally excited site defects increases with decreasing Γ , as illustrated at $\Gamma=200$ for the $N=253$

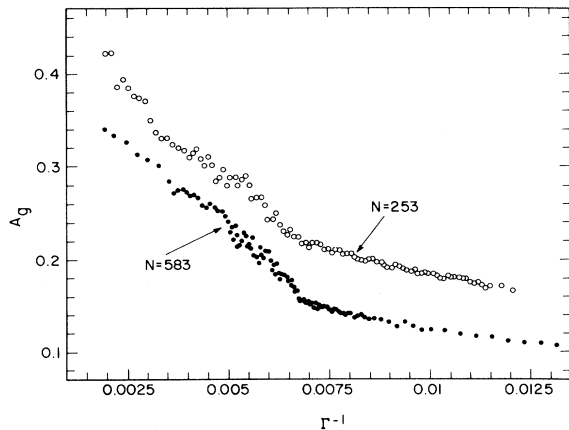


FIG. 6. Pair correlation amplitude, defined by Eq. (2.12), vs reduced temperature (Γ^{-1}) for 253- and 583-particle systems.

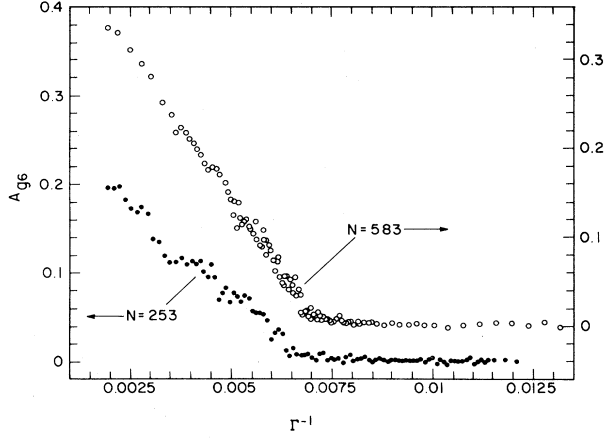


FIG. 7. Orientation correlation amplitude defined by Eq. (2.15), vs Γ^{-1} for 253- and 583-particle systems.

sample in Fig. 4 and for the $N=583$ sample in Fig. 5. Qualitatively, the length ξ_g decreases with decreasing Γ as $g(r)$ decays more rapidly. However, the simulations do not reveal a particularly characteristic value of Γ for the onset of rapid decay of $g(r)$, which might then be taken as evidence of a melting point. Transitions from algebraic to exponential decay, as predicted by theory⁴ for the asymptotic behavior at large r , are not observed. Since both $g(r)$ and $g_6(r)$ include the effects of the edges, an interpretation of the functional form of the r dependence is not attempted. Instead, the amplitudes A_g and A_{g_6} are used to characterize the simulation data.

The temperature dependence expressed as Γ^{-1} dependence, is shown for the quantities A_g , A_{g_6} , and ρ_d in Figs. 6–8, respectively. Although it is not demonstrated that the samples are equilibrated at each Γ , the simulations show that these parameters fluctuate more so with time than with small changes in Γ . Thus it was not possible to

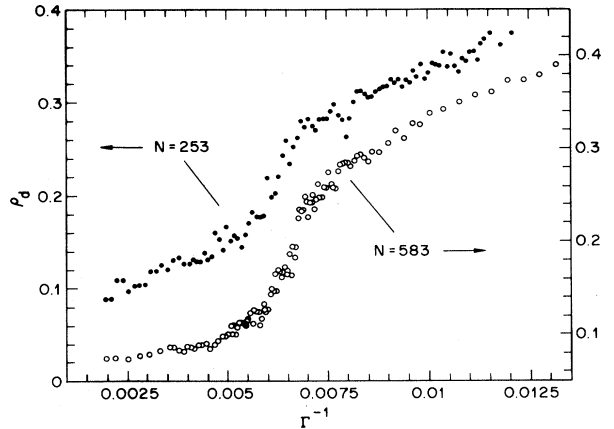


FIG. 8. Coordination defect density, defined by Eq. (2.10), vs Γ^{-1} for 253- and 583-particle systems.

discern evidence for thermal hysteresis. The data presented are the results of a series of isothermal runs taken as a function of increasing Γ^{-1} . For clarity in the display and to provide some statistical averaging, the points in the figures are averages over three runs, each of duration $1024\Delta t$.

Both samples exhibit decreasing order and greater defect density with increasing Γ^{-1} . The larger sample is more ordered for any given Γ . A pronounced change in behavior occurs at $\Gamma=148$ for the $N=583$ sample, where the Γ^{-1} dependence of A_g , A_{g_6} , and ρ_d show a fairly abrupt change in slope. This break is more smeared out for the $N=253$ sample, where it is shifted to about $\Gamma\sim 153$. This is the only noticeable feature found in the Γ^{-1} dependence. Statistical noise masks discerning possibly subtler features at lower Γ^{-1} . For higher Γ^{-1} the fluctuations are much less, and the Γ^{-1} dependences are all comparatively smoother. The transition will be labeled with the notation $\Gamma=\Gamma_I$, anticipating its identification with the onset of the isotropic fluid phase. There is no obvious precursor melting point.

Particle motion also changes at Γ_I . An elementary quantity for analysis is self-diffusion. Because of the finite geometry, the self-positional correlation function increases unbounded with time at all finite Γ . Thus the difference between particle motion in solid versus liquid phases is distinguished by the time scales, which ideally differ by a factor of N . For the finite running times used in the simulations, one measure of particle diffusion is the variance in particle displacements. The following parameter is used:

$$\chi^2 = (m\sigma^2)^{-1} \sum_i |\vec{r}_i(m\Delta t) - \vec{r}_i(0)|^2, \quad (3.1)$$

where the net displacements over the duration of a run of m time steps is used in the computation. Results are shown in as a function of Γ^{-1} in Fig. 9. In addition to the expected increase of χ^2 with Γ^{-1} , an abrupt change in behavior occurs at Γ_I and is found for both samples.

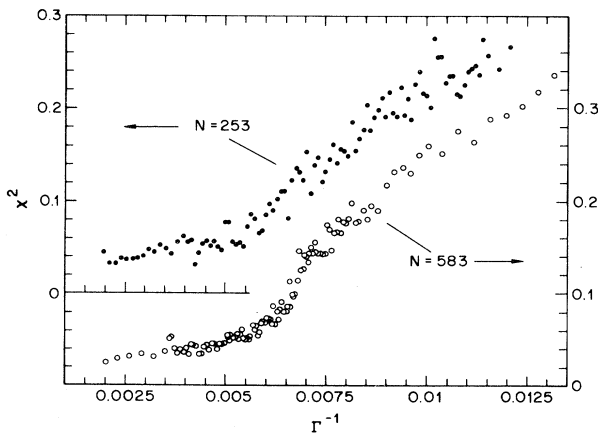


FIG. 9. Normalized mean-square particle displacements, defined by Eq. (3.1), vs Γ^{-1} .

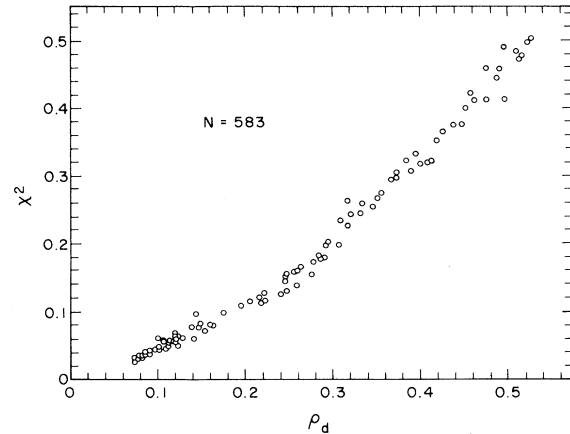


FIG. 10. Normalized mean-square particle displacement vs defect density, implicit functions of Γ , for the 583-particle system.

Though the parameter χ^2 is poorly defined for low Γ^{-1} , where it decreases with m , it is nevertheless useful for exhibiting trends. In addition, it is found that χ^2 does not simply scale or increase with the density of site defects, as shown in Fig. 10, where χ^2 is plotted against ρ_d for the $N=583$ sample. This plot shows a change in slope in the vicinity of $\rho_d=0.25$, which corresponds to $\Gamma=\Gamma_I$, indicating a change in microscopic dynamical behavior.

Further interesting information is the manner in which the site defects form clusters. This is shown in Figs. 11 and 12, where plotted against Γ^{-1} are the quantities $\langle r_l^2 \rangle$ and $\langle r_u^2 \rangle$, which are mean-square nearest-neighbor spacings between site defects of like kind (e.g., 5-5 and 7-7 pairs) and unlike kind (5-7), respectively. The lengths have been normalized to the triangular lattice parameter a , given by

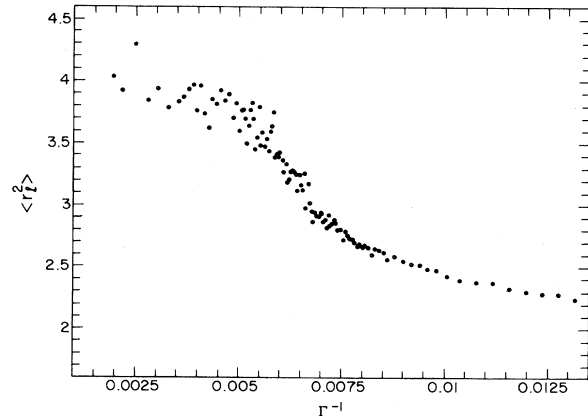


FIG. 11. Mean-square separation in units of interparticle spacing between (5-5) or (7-7) neighboring coordination defect pairs vs Γ^{-1} for the 583-particle system.

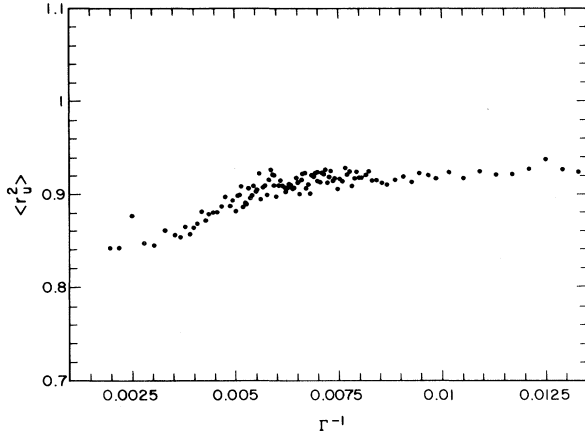


FIG. 12. Mean-square separation between (5-7) and other dissimilar neighboring coordination defect pairs vs Γ^{-1} for the 583-particle system.

$$a^2 = 2(3^{-1/2})N^{-1}\pi R^2. \quad (3.2)$$

The 5-7 spacing at low Γ^{-1} approaches $\langle r_{ij}^2 \rangle \sim 3^{1/2}a^2/2$, since the dominant defects are dislocations. However, the ratio $\langle r_{ij}^2 \rangle / \langle r_u^2 \rangle$ at low Γ^{-1} is much larger than a value ~ 2 , expected if all of the defects were closely paired dislocations, a square 5-7-5-7 formation. For such a configuration, the dislocations are displaced parallel to their Burgers vectors. The observed ratios fall between 3.4 and 4.4 in the region $\Gamma^{-1} < \Gamma_I^{-1}$, indicating that there are dislocations which are further apart. For example, a dislocation pair displaced perpendicular to the Burgers vectors, a 5-7-5-7 in-line string, gives $\langle r_u^2 \rangle \sim 4$.

At temperatures near Γ_I , the fraction of site defects has become large enough that clusters and networks form. From visual inspection of various particle configurations one finds separated dislocations, dislocation pairs, strings

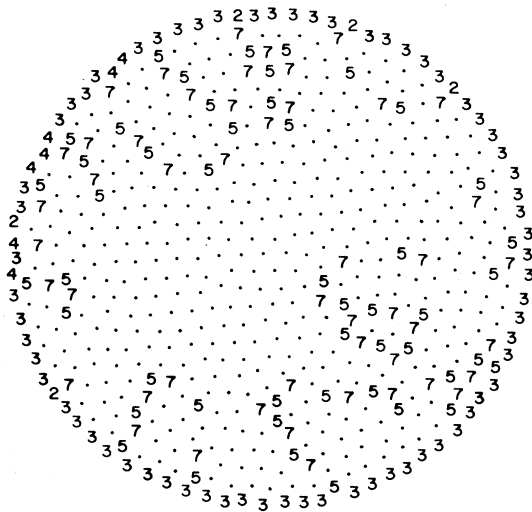


FIG. 13. Particle configuration at $\Gamma = 149 > \Gamma_I$ for a $N = 583$ sample.

of site defects which resemble crystallite-grain boundaries, as well as denser clusters. Thus there is no one defect pattern which could be identified with a mechanism driving the disorder. For illustration, a configuration is shown in Fig. 13 for $\Gamma = 149$, which is just below (cooler) the Γ_I transition and in Fig. 14 for $\Gamma = 143$, which is just above (warmer) Γ_I . Similar complexity of the defect configurations near melting has been found in other simulations, where periodic boundary conditions are used.^{1,20} Figure 11 shows that $\langle r_{ij}^2 \rangle$ approaches 2 at large Γ^{-1} , as the higher density defect clusters form more closely packed arrangements.

The transition region $\Gamma \sim \Gamma_I$ is displayed in more detail in Figs. 15 and 16 where $g(r)$ and $g_6(r)$ are, respectively, plotted for three values of Γ . The $g(r)$ function is strongly damped in this region, as evident in all three parts of Fig. 15. Even for $\Gamma > \Gamma_I$, Fig. 15(a), $g(r)$ decays to a small value at $r \sim R$, indicative of liquidlike positional order. Upon heating through Γ_I , the decay length ξ_g decreases from 0.20R at $\Gamma = 149$ to 0.12R at $\Gamma = 145$. The fluctuations create uncertainty in these quantities of about 20%.

Qualitative changes in $g_6(r)$ at Γ_I are more dramatic than for $g(r)$. The curve for $\Gamma > \Gamma_I$ in Fig. 16(a) is similar in shape to the low-temperature results, Fig. 3, in so far as the decay of $g_6(r)$ is long range, extending beyond the radius of the disc. The main difference between Fig. 3 and Fig. 16(a) is that the magnitude of $g_6(r)$ is depressed at the lower Γ . The behavior shown in Figs. 15(a) and 16(a) is qualitatively like the hexatic liquid crystalline phase postulated theoretically by Nelson and Halperin⁴ and is similar to that found by McTague *et al.* in a Leonard-Jones system.²⁰ Although Fig. 15(a) shows that the system is not a solid, it cannot necessarily be concluded from Fig. 16(a) alone that orientational order is stable, i.e., that $g_6(r)$ decays algebraically.⁴

Rapid decay of $g_6(r)$ is found for $\Gamma < \Gamma_I$ as displayed in Fig. 16(c). Indeed the orientational order does not persist beyond $r \sim R$. There is a greater tendency towards boundary alignment, as evident by sharper peaks in $g_6(r)$ near

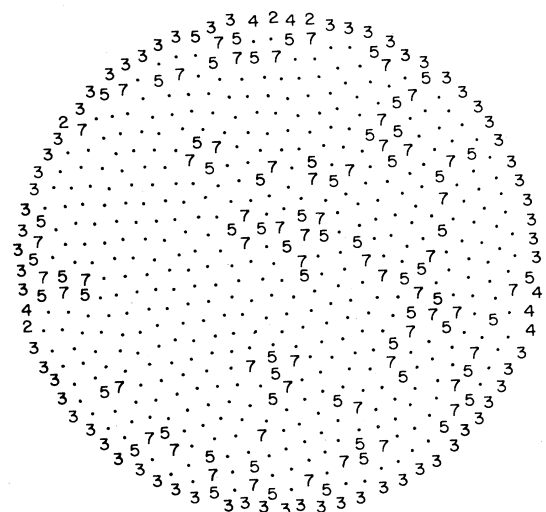


FIG. 14. Particle configuration at $\Gamma = 143 < \Gamma_I$ for a $N = 583$ sample.

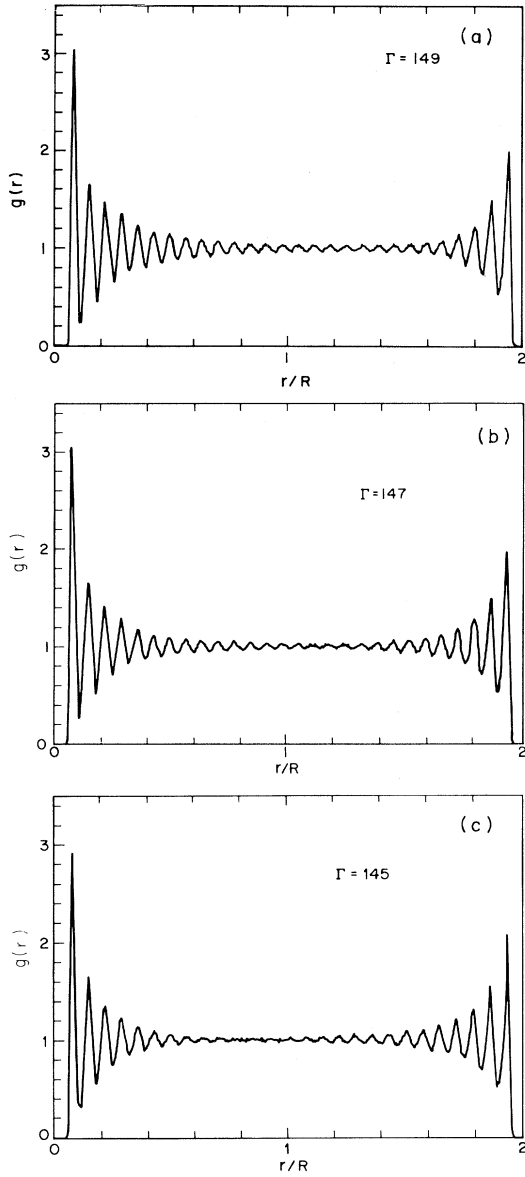


FIG. 15. Pair correlation function at three Γ values near Γ_I . (a) 149, (b) 147, (c) 145.

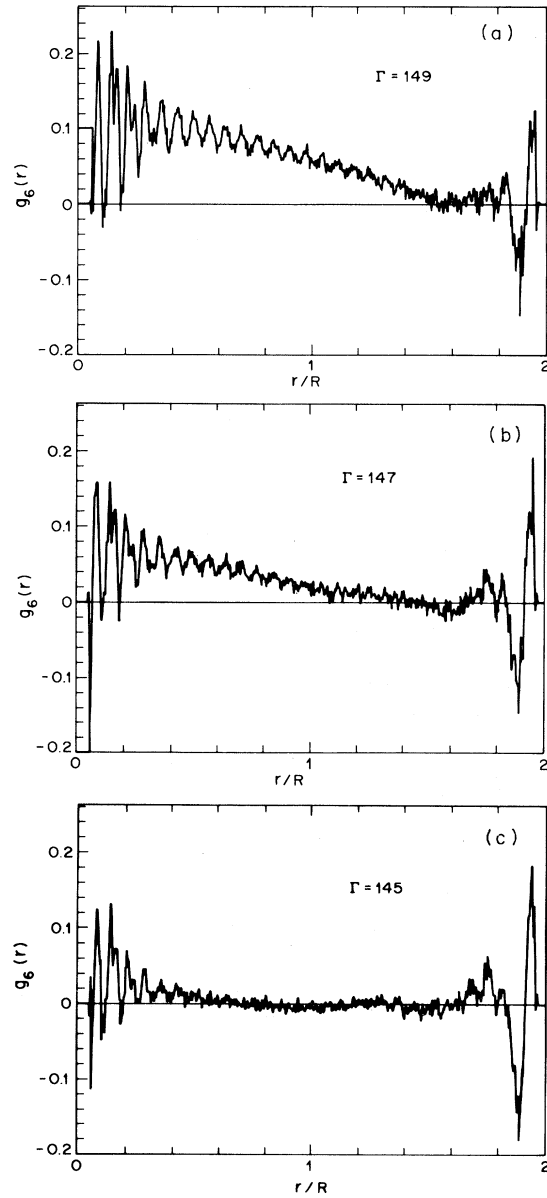


FIG. 16. Orientational-order correlation function at three values of Γ near Γ_I . (a) 149, (b) 147, (c) 145.

$r \sim 2R$. It is clear, therefore, that in the $\Gamma < \Gamma_I$ region the system is like an isotropic liquid exhibiting short-range order in both $g(r)$ and $g_6(r)$. Previous work has shown that short-range fluid order persists up to $\Gamma = 4$ in the one-component plasma phase.^{2,3}

The quantity χ^2 presented earlier is a macroscopic average over all particle displacements. However, inspection of individual particle trajectories reveals that the displacements are spatially inhomogeneous in the vicinity of the Γ_I transition. For $\Gamma > \Gamma_I$ it is possible to identify correlated regions of size comparable to ξ_g which, with time, slip with respect to one another. Particles at the slip boundaries undergo larger than average displacements. However, in other regions of the sample, there are more

compact clusters of particles with above-average displacements.

The change in potential energy per particle at Γ_I found for the $N=583$ system is $0.0007(6)q^2$, which implies an entropy change $\Delta S/k_B = 0.10(9)$. Although the uncertainty is large, ΔS is clearly much less than the entropy of melting of $0.4k_B$ found in the same Γ region by Monte Carlo² and $0.36k_B$ from molecular dynamics.³ On comparing the $N=583$ crystal at $\Gamma=500$ and the isotropic fluid at $\Gamma=145$, a potential energy change of $0.0084(4)q^2$ is found. For comparison, the potential energy change computed from results presented by de Leeuw and Peram, between crystalline and fluid phases extrapolated to similar values of Γ , is $0.0082q^2$, which includes a latent

heat of $0.0027q^2$ in the vicinity of $\Gamma=135$. Thus Brownian-motion dynamics and molecular dynamics produce the same result for this crystal-liquid potential energy difference. The essential difference is that the present Brownian-dynamics results are consistent with $\Delta S=0$ at Γ_I . These systems exhibit negligible thermal expansion. The area as measured by $\langle r_i^2 \rangle$ is constant to two parts in 10^4 in the range $\Gamma \gtrsim \Gamma_I$.

IV. CONCLUSIONS

Brownian-motion simulations of Coulomb particles confined within finite discs show a well-marked transition to an isotropic fluid at $\Gamma_I \sim 148$ for a $N=583$ particle system. In the region $\Gamma > \Gamma_I$ the system appears as an orientationally ordered liquid, perhaps a hexatic phase. Presumably the bend stress imposed by the boundary depresses the transition temperature, since Γ_I increases with smaller N . It was not possible to reveal another melting transition of the finite crystal at larger Γ . For comparison, the molecular dynamics results of de Leeuw and Perram³ show a hysteretic transition for $\Gamma \approx 135$, while Caillol *et al.*² have inferred that a transition is located at $\Gamma \approx 140$. Fisher's theory for vortex lattices predicts melting in a range of Γ from 120 to 220.¹⁷

Energy considerations are ambiguous as to whether the Γ_I transition is thermodynamically second order since the

systems are of finite size. However, it should be possible to test the dynamics of the transition by imposing shear and bend perturbations and establishing the time dependence. The features of a second-order transition such as critical slowing down and divergent correlation lengths are expected to be cut off by the finite R . Thus the maximum relevant times are those for the diffusion of dislocations and disclinations over distances comparable to $2R$. These were not determined in the present work. However, the motion of dislocations in vortex lattices in superconductors was treated theoretically by Brandt²¹ and by Kramer.²² For glide motion, dislocations can move on the order of N times faster than the individual particles. Hence this is a possible mechanism for relaxing long-range ($r \sim R$) order in the disc for the running times used in the present simulation.

Another area for further investigation is to increase the sample size and examine $g(r)$ and $g_6(r)$ for only a center portion of the sample. This was not done here because $N=583$ was deemed too small to allow a reasonable size for the truncated specimen.

ACKNOWLEDGMENTS

The author benefitted from discussions with D. S. Fisher, G. H. Gilmer, A. F. Hebard, D. R. Nelson, and J. D. Weeks.

¹See J. Q. Broughton, G. H. Gilmer, and J. D. Weeks, *Phys. Rev. B* **25**, 4651 (1982), and references therein; also, W. F. Brinkman, D. S. Fisher, and D. E. Moncton, *Science* **217**, 693 (1982); *Symposium on Melting, Localization and Chaos*, edited by R. K. Kalia and P. Vashishta (North-Holland, Amsterdam, 1982); *Ordering in Two Dimensions*, edited by S. K. Sinha (North-Holland, Amsterdam, 1980).
²J. M. Caillol, D. Levesque, J. J. Weis, and J. P. Hansen, *J. Stat. Phys.* **28**, 325 (1982).
³S. W. de Leeuw and J. W. Perram, *Physica* **113A**, 546 (1982).
⁴D. R. Nelson and B. I. Halperin, *Phys. Rev. B* **19**, 2457 (1979).
⁵J. M. Kosterlitz and D. J. Thouless, in *Progress in Low Temperature Physics*, edited by D. Brewer (North-Holland, Amsterdam, 1978), Vol. VIIb, Chap. 5.
⁶S. T. Chui, in *Melting, Localization and Chaos*, edited by R. K. Kalia and P. Vashishta (North-Holland, Amsterdam, 1982).
⁷T. V. Ramakrishnan, *Phys. Rev. Lett.* **48**, 541 (1982).
⁸R. Morf, *Phys. Rev. Lett.* **43**, 931 (1979).
⁹J. Tobochnik and G. V. Chester, in *Ordering in Two Dimensions*, edited by S. K. Sinha (North-Holland, Amsterdam,

1980), p. 339.

¹⁰A. Zippelius, B. I. Halperin, and D. R. Nelson, *Phys. Rev. B* **22**, 2514 (1980).

¹¹P. Dutta and S. K. Sinha, *Phys. Rev. Lett.* **47**, 50 (1981).

¹²A. L. Fetter and P. C. Hohenberg, *Phys. Rev.* **159**, 330 (1967).

¹³R. E. Packard, *Physica* **109-110B+C**, 1474 (1982).

¹⁴J. Pearl, in *Low Temperature Physics—LT9*, edited by J. G. Daunt, D. O. Edwards, F. J. Milford, and M. Yagub (Plenum, New York, 1965), p. 506.

¹⁵E. Conen and A. Schmid, *J. Low Temp. Phys.* **17**, 331 (1974).

¹⁶B. A. Huberman and S. Doniach, *Phys. Rev. Lett.* **43**, 950 (1979).

¹⁷D. S. Fisher, *Phys. Rev. B* **22**, 1190 (1980).

¹⁸A. F. Hebard and A. T. Fiory, *Physica* **109-110B**, 1637 (1982).

¹⁹L. J. Campbell and M. Ziff, *Phys. Rev. B* **20**, 1886 (1979).

²⁰J. P. McTague, D. Frenkel, and M. P. Allen, in *Ordering in Two Dimensions*, edited by S. K. Sinha (North-Holland, Amsterdam, 1980), p. 147.

²¹E. H. Brandt, *Phys. Status Solidi* **36**, K167 (1969).

²²E. J. Kramer, *J. Appl. Phys.* **41**, 621 (1970).